

Article

Fusion of Remotely-Sensed Fire-Related Indices for Wildfire Prediction through the Contribution of Artificial Intelligence

Nikolaos Ntinopoulos ¹, Stavros Sakellariou ^{1,*} , Olga Christopoulou ¹  and Athanasios Sfougaris ²

¹ Department of Planning and Regional Development, University of Thessaly, 38334 Volos, Greece; nntinopoulos@uth.gr (N.N.); ochris@uth.gr (O.C.)

² Department of Agriculture Crop Production and Rural Environment, University of Thessaly, 38446 Volos, Greece; asfoug@agr.uth.gr

* Correspondence: stasakel@uth.gr

Abstract: Wildfires are a natural phenomenon, which nowadays, due to the synergistic effect of increased human intervention and the escalation of climate change, are displaying an ever-increasing intensity and frequency. The underlying mechanisms present increased complexity, with the phenomenon itself being characterized by a significant degree of stochasticity. For the above reasons, machine learning models and neural networks are being implemented. In the current study, two types of neural networks are implemented, namely, Artificial Neural Networks (ANN) and Radial Basis Function Networks (RBF). These neural networks utilize information from the Fire Weather Index (FWI), Fosberg Fire Weather Index (FFWI), Normalized Difference Vegetation Index (NDVI) and the Normalized Difference Moisture Index (NDMI), aiming to predict ignitions in a region of Greece. All indices have been developed through the Google Earth Engine platform (GEE). In addition, a new index is proposed named “Vegetation-Enhanced FWI” (FWIveg) in order to enhance the FWI with vegetation information from the NDVI. To increase the robustness of the methodology, a genetic algorithm-based approach was used in order to obtain algorithms for the calculation of the new index. Finally, an artificial neural network was implemented in order to predict the Mati wildfire in Attica, Greece (23 July 2018) by applying the new index FWIveg, aiming to assess both the effectiveness of the new index as well as the ability to predict ignition events using neural networks. Results highlight the effectiveness of the two indices in providing joint information for fire prediction through artificial intelligence-based approaches.

Keywords: wildfires; neural networks; FWI; NDVI; Greece; Google Earth Engine



Citation: Ntinopoulos, N.; Sakellariou, S.; Christopoulou, O.; Sfougaris, A. Fusion of Remotely-Sensed Fire-Related Indices for Wildfire Prediction through the Contribution of Artificial Intelligence. *Sustainability* **2023**, *15*, 11527. <https://doi.org/10.3390/su151511527>

Academic Editor: Maxim A. Dulebenets

Received: 28 June 2023
Revised: 20 July 2023
Accepted: 22 July 2023
Published: 25 July 2023



Copyright: © 2023 by the authors. Licensee MDPI, Basel, Switzerland. This article is an open access article distributed under the terms and conditions of the Creative Commons Attribution (CC BY) license (<https://creativecommons.org/licenses/by/4.0/>).

1. Introduction

Forests are considered a vital resource [1] since they are an environmental health indicator of a region [2], while also functioning as carbon sinks with a concentration capacity of 66% of the total earth surface carbon [3]. Forest ecosystems can significantly contribute to the global economic sector [4]. Urbanization and industrialization have led to a total loss of forest habitat of about 32%, with forest fires contributing even more to the phenomenon [5].

Forest fires are a natural phenomenon for many ecosystems, especially in the Mediterranean basin [6,7]. When ignition patterns follow a normal frequency and present normal intensities, they naturally contribute to the burn of dead matter and parasites. At the same time, they can also enrich the soil with nutrients from the burnt biomass and free up space and sunlight paths. Parameters related to wildfires, such as meteorological variables, have been proven to influence the population density of various species, which can be characterized as an additional ecosystem quality index [8].

Nowadays, wildfires have been amplified by global climate change [9], with increasing temperatures and prolonged droughts leading to ever-increasing fire intensities [10]. The

climate and meteorology of a region have been proven to be the leading factors affecting both fire occurrence and spread [11] since the meteorological characteristics influence fuel availability and features [12]. A major part of the Mediterranean region, as well as that of Greece, has been deemed quite vulnerable regarding climate change, with the latter having experienced four major drought incidents during the mid-1970s, the end 1980s and the start of the decades 1990 and 2000 [13].

In order to quantify relationships of the above mechanisms, a common practice includes the determination of the so-called “Fire Indices”, such as the Canadian Fire Weather Index (FWI). A better understanding of wildfires and their underlying mechanisms could lead to significant resource savings due to the optimization of fire management [14–16].

The acquisition of satellite data through remote sensing can pose an important tool in environmental studies, especially in the case of wildfires [17], since it allows the acquisition of continuous multi-level information of a specific study region, eliminating the information loss that would come from specific points such as meteorological stations or modeled points. Having obtained the most reliable data possible, there are various methods that have been implemented for the study of wildfires, such as logistic regression and machine learning models [18–21]. The most representative indices frequently used are the FWI [22–24] and the Normalized Difference Vegetation Index (NDVI), which can provide direct and indirect information about vegetation attributes as well as fuel characteristics. Another frequently used Fire Index in the Mediterranean [25–27] and other ecosystems constitute the Fosberg Fire Weather Index (FWI). All the mentioned indices—despite their effectiveness in fire danger classification—are not directly correlated with fire occurrence itself due to the randomness associated with the phenomenon. This problem is tackled with the use of neural networks, which can handle high volumes of data and derive information that would be impossible to manually obtain, while also being impossible to be obtained by deterministic models [28].

Many authors have used neural networks for several purposes concerning wildfires. For instance, Zhang et al. [29] used Faster R-CNN for the detection of smoke in satellite images. Jeong et al. [30] used a hybrid solution of Long Short-Term Memory (LSTM) and You Only Look Once (YOLO) for the detection of smoke during wildfires. In a study by Srinivas et al. [31], a Convolutional Neural Network (CNN) was used for the detection of fires in satellite images. Neural networks have also been used for the geolocation of wildfires [30,32–34], while Cao et al. [35] used a new method called “Attention-enhanced Bidirectional Long Short-Term Memory” (Abi-LSTM) for wildfire classification. Govil et al. [36] proposed a fire detection scheme with the development of cameras and binary image classification in “smoke/no-smoke” categories, taking advantage of an image recognition model (Inceptionv3) from Google with a proven accuracy of 78.1%. In the study of Lai et al. [37], a neural network approach was implemented for fire prediction in the region of Montesinho Natural Park, Portugal, with the approach yielding a Root Mean Squared Error (RMSE) of 0.95–19.3. Zheng et al. [38] used a Deep Convolutional Network (DCNN) for the acquisition of image attributes and fire danger forecasting, while Bisquert et al. used an ANN approach with remote sensing data as input to perform fire danger classification for the region of Galicia of Spain [39]. A slightly different approach was used by Joshi et al. [40], who used an Artificial Neural Network (ANN) for burnt area prediction on a global scale. Kucuk et al. [41] implemented an artificial neural network and a decision tree to model fire spread as well as intensity in pine (*Pinus nigra* Arnold) forests in Türkiye. Pais et al. [42] were able to quantify the influence of surface topology on wildfires and achieve fire prediction through the use of neural networks in south-central Chile. In the study of Abdollahi et al. [43], an “explainable intelligence” model called Shapley additive explanations (SHAP) was implemented to interpret the results of a deep learning model that was used for fire prediction in Australia. A Deep Learning Neural Network (DLNN), used by Saha et al. [44] in order to classify fire danger zones in the Ayodhya hill region in India, achieved an accuracy assessed as the Area Under the Curve (AUC = 0.925). Finally, Permana et al. [45] used a deep learning algorithm and a Convolutional Neural Network

(CNN) to classify bird sounds in order to predict fire incidence in Indonesia. Bird sounds were classified into two categories, one being normal circumstances and the other under normal or panic conditions, with the CNN achieving an accuracy of 96.45%.

The novelty and added value of the paper are two-fold. Two types of neural networks have been developed, namely, an Artificial Neural Network (ANN) and a Radial Basis Function (RBF) for the prediction of ignitions, deriving information from fire (FWI, FFWI) and remote sensing indices (NDVI, NDMI). This process exploited the Google Earth Engine (GEE) capabilities. The pilot study area is the broad region of Greece, analyzing time-series data for the fire season, namely from March to October (2019–2022). Secondly, a new index named “Vegetation-Enhanced Fire Weather Index” (FWIveg) is proposed deriving from the combination of the FWI and the NDVI in order to contain both weather and vegetation favorability information about wildfires. The calculation of the new index is achieved through the use of genetic algorithms. A new ANN was tasked with predicting the fire in the case of Mati-Attica (23 July 2018), by assessing the similarity of fire incidents with other fires based on the profile of the components of the new index. This index can be used for estimating future wildfires and optimizing fire prevention and management.

2. Materials and Methods

2.1. Study Region

The study areas include the entire country for the first part of the methodology and the region of Attica for the second part (Figure 1). The Greek climate, being classified as a Mediterranean ecosystem, exhibits dry winters, with water shortages during the annual cycle [46]. The climate ranges from continental Mediterranean on the northern part to subtropical in the southernmost edges of the country, with intense shifts from one category to the other being noticed from the continental toward the coastal parts of the country [47]. The increased climatic variability noted in the Greek domain can be mainly attributed to the effects of topography and aerial masses coming from the central part of the Mediterranean. As a result, the western part of the country tends to be wetter, while the eastern part is hotter and drier. It has been observed that in Mediterranean ecosystems, climate variability is the leading factor regarding wildfire seasonality and fuel layer flammability [48]. Increased fuel flammability due to prolonged drought and higher overall temperatures is considered one of the main ecosystem responses to climate change [49].

2.2. Data Preprocessing

Multiple types of data have been used for the purposes of this study. Precipitation data were obtained by the CHIRPS (“Climate Hazards group Infrared Precipitation with Stations”) dataset. The CHIRPS dataset combines precipitation estimates through Cold Cloud Duration (CDD) estimates based on satellite observations of 0.05° , coupled with in situ observations from meteorological stations.

The MOD09GA.061 product of the MODIS satellite is a dataset with modeled reflectance values on a daily basis. Due to the MODIS satellite’s temporal resolution being 8 days, modeled values for the intermediate periods can increase temporal resolution and provide more detailed insights regarding the data. The dataset has been corrected for atmospheric scattering, aerosols and aerial gases. The spatial resolution for the reflectance bands is 500 m, corresponding to the following spectral ranges: 1 (620–670 nm), 2 (841–876 nm), 3 (459–479 nm), 4 (545–565 nm), 5 (1230–1250 nm), 6 (1628–1652 nm) and 7 (2105–2155 nm). The dataset was implemented after cloud, cirrus and shadow pixels were masked.

The CFSR (Climate Forecast System Reanalysis) dataset possesses values for climatic variables, such as air temperature, relative humidity, wind speed and others. It has global coverage and a spatial resolution of ~ 38 km (T382) with 64 fields. The dataset has been produced by the coupling of atmosphere, ocean, land surface and sea ice systems to provide estimates of climate variables in six-hour guess fields [50].

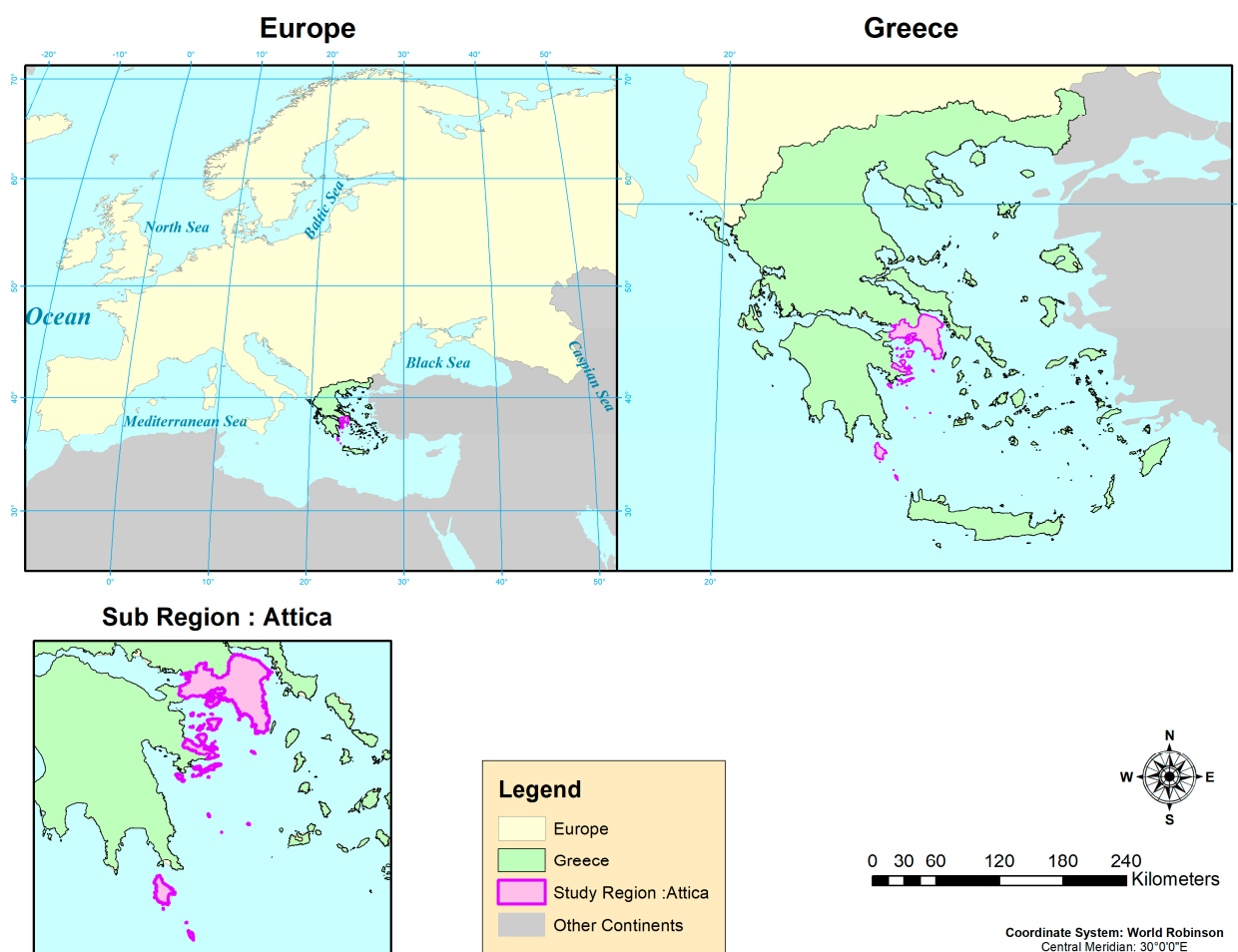


Figure 1. Geographical location of the study area in European, National and Regional context.

For the monitoring of wildfires, the FIRMS (Fire Information for Resource Management System) dataset (<https://www.earthdata.nasa.gov/learn/find-data/near-real-time/firms> (accessed on 27 June 2023)) was used. The FIRMS dataset bears observations for historical and active fires detected by the Moderate Resolution Imaging Spectroradiometer (MODIS) satellite by acquiring the brightness temperature for each pixel in K° to account for thermal anomalies. The dataset has a spatial resolution of 1 km. Areas that present active fires are detected through MODIS instruments and are then processed by LANCE. The final result is rectangular centroids/bounding boxes of 1 km spatial resolution in which one or more fires are expected to be noted. The dataset has a temporal span of 2000 till the present day on a daily basis, with areas that do not present thermal anomalies.

All indices required for the current study, as well as the detection of wildfires, were performed on Google Earth Engine (GEE). Calculations in GEE were performed in Javascript language. Further processing of results and calculations outside of GEE, as well as creation and training of all neural networks, took place in python and C++ language.

All datasets were temporally limited to the study period 2019–2022 (March–October), a period that also includes the Greek fire season (May–October). Detection and exclusion of cloud values in pixels was the first step of data preprocessing [51].

2.3. Primary Indices Estimation

2.3.1. Normalized Difference Vegetation Index (NDVI)

The NDVI (Normalized Difference Vegetation Index) is the most widespread remote sensing index used to assess vegetation state [52,53] and provide direct and indirect information about vegetation attributes. It is calculated as the normalized difference between the

reflectance in the Near-Infrared (NIR) 0.77–0.90 μm and RED spectra 0.63–0.69 μm . Index values range from -1 to 1 . Healthy vegetation, due to chlorophyll presence, exhibits high reflectance values in the NIR spectrum and much lower ones in the RED spectrum, and as a result, when the index values approach 1 , indicate healthy vegetation cover of an area, while values approaching 0 indicate unhealthy or dead vegetation. Negative NDVI values indicate presence of water in the focus region [54].

2.3.2. Normalized Difference Moisture Index (NDMI)

The NDMI index, according to McFeeters et al. [55], is calculated as the normalized difference between the NIR and the GREEN band. The term GREEN refers to the reflectance in the green spectrum (“sur_refl_b04”) 0.545–0.565 μm , while NIR refers to the reflectance in the near-infrared spectrum. Values of the index greater than zero indicate water presence, while zero or negative values depict soil features. This is attributed to the higher reflectance of water in the GREEN spectrum compared to the NIR, with the opposite being true for soil [54].

2.3.3. Fosberg Fire Weather Index (FFWI)

The FFWI index is a fire index that uses information about air temperature (T), wind speed (U) and relative humidity (Rh). The index presents simplicity of calculation while its effectiveness has been proven in its ability to accurately classify fire danger in Mediterranean and other types of ecosystems [29–31,56]. Values of the index present non-linear relationships between the composing variables of wind speed, temperature and decreases in relative humidity. The range of values is 0 to 100 and increases proportionally with fire danger, with a value of 100 corresponding to $U = 30$ mph and $Rh = 0\%$. [36].

2.3.4. Fire Weather Index (FWI)

The Canadian Fire Weather Index (FWI) was developed by van Wagner et al. [57] and is a fire index with values ranging from zero to infinity, indicating an ever-increasing fire danger. It is comprised of five sub-indices called codes. Three moisture codes, namely the Fine Fuel Moisture Code (FFMC), Duff Moisture Code (DMC) and Drought Code (DC), assess moisture content in increasing depths of the fuel beds. The latter two codes are fire behavioral indices. The Initial Spread Index (ISI) assesses fire spread potential during its initial stages, and the Buildup Index (BUI) assesses fuel availability by combining the DMC and DC. Due to the increased complexity of the fire weather index calculations [57], the index was not directly computed in GEE; instead, meteorological variables were obtained for a bounding box of the study region. What followed was the implementation of a Poisson model following the methodology of Ntinopoulos et al. [58] in order to acquire an exponential relationship between the FWI values and its components that would be used in GEE to calculate the FWI.

2.4. Implementation of Neural Networks

A total of 100 random points within the study region were selected and were then split into categories (fire and no fire). Each point had 13 attributes (i.e., minimum, median and maximum values of all the mentioned indices as well as the number of ignitions). Two types of neural networks, an Artificial Neural Network (ANN) and a Radial Basis Function (RBF) network, were constructed for fire prediction using as input the index values of these points.

2.4.1. Implementation of Artificial Neural Network (ANN)

In the case of ANN (Figure 2), calculations are linear: $Y = W \times X + B$, where X , Y represent the input and output. The terms W , B represent the weights and biases that have to be applied to X in order to produce results that, after consecutive propagations, will predict the output Y as accurately as possible ($Y_{\text{predicted}} \cong Y_{\text{actual}}$). In our case, the output Y represents the number of ignitions per point and has dimensions $(100,1)$. The

input's X dimensions are (100,12). Apart from the W,B parameters, neural network layers also utilize various functions to limit the values of the results within a desired range. These functions are called activation functions. In the current case, the sigmoid function was used, which limits values in the range [0, 1].

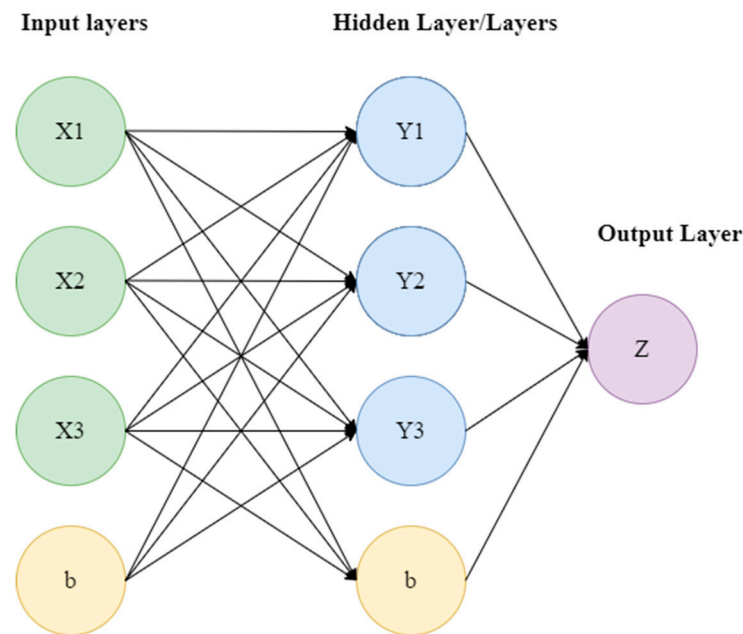


Figure 2. Schematic representation of the function of an ANN. The input layer (X) feeds—along with its bias—the hidden layers that produce a result and consecutively propagates it to the next layers until the final output layer.

Initiation of W, B matrix values is random, so the initial $Y_{\text{predicted}}$ is inaccurate. Calibration of the W and B will be facilitated through repetitive cycles—epochs of forward and backward propagation based on the prediction error $E = \sum (Y_{\text{actual}} - Y_{\text{predicted}})^2$.

A parameter called learning rate is a positive < 1 constant that determines the “calibration step” of the network parameters. In the current study, the learning rate was defined as 0.01 for all layers.

The entire dataset was segmented into 10 batches of 10 points each. The nine first batches were used to train the network and find the optimal W, B parameters. Then, for the tenth testing batch, predictions were made by using the parameters of all nine batches to find which set of parameters produces predictions that better approximate the actual Ystate based on cumulative error. Five layers were used for the ANN, which was trained for different numbers of epochs (100, 500, 1000, 10,000, 25,000).

As a first metric of accuracy of the ANN prediction, the Mean Absolute Error (MAE) was calculated between predictions through parameters coming from each of the 9 training batches and the actual state of the 10th batch, according to Equation (1).

$$\text{MAE} = \sum_{i=0}^n (|Y_{\text{actual}} - Y_{\text{predicted}}|) / n \quad (1)$$

To select the optimal number of epochs, the criterion used was the return period of $\text{MAE} > 0.25$ (T_{MAE}), signifying the number of epochs after which the MAE would surpass the value of 0.25. The threshold for the MAE value was selected since it can be deemed high compared to the error during the end of the training phase, which is two orders of magnitude lower. The final MAE was also assessed for each number of epochs.

2.4.2. Implementation of Radial Basis Network (RBF)

An RBF network was also used, tasked with performing supervised classification of the points. In our case, the known categories are fire and no fire. The classification was performed based on the distance of each point from the center of mass of each category. The distance was calculated by the radial basis function, as shown in Equation (2).

$$\varphi = \exp(-r^2/2\sigma^2) \quad (2)$$

where r is the Euclidean distance, and σ is the standard deviation. The vector of the two categories is [fire, no fire]; hence, actualization of each condition is expressed by the vector, taking the value of 1 in the specific condition and 0 in the opposite.

$$\begin{aligned} [1, 0] &\Rightarrow \text{fire} \\ [0, 1] &\Rightarrow \text{no fire.} \end{aligned} \quad (3)$$

After the vector of distances $\Phi_i = [\varphi_1, \varphi_2]$ ($\varphi_1, \varphi_2 \in [0, 1]$) was calculated for each point, the aim of the network was to train itself to obtain the optimal W, B parameters for the distinction between the two categories to be as clear as possible leading to distinct classification (as expressed in Equation (3)). The distance was calculated between the points and the known centers of mass of the two categories.

The network used 50 points in 5 10-point batches. Four of those batches were used for training the network, and the final one was used for predictions with the parameters coming from the training of all 4 training batches, similar to Section 2.4.1. The learning rate was set to 0.01 and the epoch number to 200.

The criteria to find the best-performing batch parameters were the mean absolute error during the testing phase. The error matrix (4) was composed having values of the errors of the predictions. Each row i corresponds to the error of predictions made based on the parameters of the i th batch.

$$\text{Error Matrix} = \begin{bmatrix} \text{Error using parameters of batch 0} \\ \vdots \\ \text{Error using parameters of batch } n = 4 \end{bmatrix} \quad (4)$$

2.5. General Assessment of Neural Networks, Applying the ROC (Relative Operating Characteristic) Method

The Relative Operation Characteristic (ROC) method was used in order to assess the accuracy of binary classification methods (Neural Networks, Machine Learning Methods, etc.). The method is based on the categorization of observations into four groups, those being True Positive (TP), False Positive (FP), True Negative (TN) and False Negative (FN) [59]. For the current study, the mentioned terms are interpreted as follows:

- True Positive (TP): Each time the neural network correctly predicts ignition.
- False Positive (FP): Each time the neural network incorrectly predicts ignition.
- True Negative (TN): Each time the neural network correctly predicts non-ignition.
- False Negative (FN): Each time the neural network incorrectly predicts non-ignition.

The terms True Positive Rate (TPR) and False Positive Rate (FPR) assess the total number of correctly and incorrectly predicted ignitions divided by the number of total actual ignitions and total actual non-ignitions accordingly.

$$\text{TPR} = \text{TP}/(\text{TP} + \text{FN}) \quad (5)$$

$$\text{FPR} = \text{FP}/(\text{FP} + \text{TN}) \quad (6)$$

2.6. Vegetation Enhanced Fire Weather Index

Despite its effectiveness in classifying fire danger, the FWI does not account for the vegetation state of a region, which is a proxy of the fuel attributes, a factor that can greatly affect fire danger. In order to enrich the FWI, the Vegetation Health Index (VHI) [60] was used, which combines two additional indices, the VCI and TCI, according to Equation (7).

$$\text{VHI} = \alpha \cdot \text{VCI} + (1 - \alpha) \cdot \text{TCI} \quad (7)$$

The VCI (Vegetation Condition Index) expands upon the NDVI [61], assessing meteorological effects on vegetation health. It compares the current NDVI value with the minimum and maximum one for the study period in the examined region. It is calculated according to Kogan et al. [62], with its values ranging from 0 to 100, indicating a proportional increase in vegetation health. The TCI (Temperature Condition Index) [54] is based on a similar logic and assesses temperature stress of vegetation. It is based upon satellite observations of the Land Surface Temperature (LST) and also ranges from 0 to 100, indicating an inversely proportional relationship between vegetation health.

The parameter α of Equation (7) received the value of 0.5, similar to the case of Masitoh et al. [63]. Following the logic of the VCI and TCI indices, a new index, FWI_CI (“Condition Index”), was developed in order to acquire information about FWI variations instead of only having its numerical value.

$$\text{FWI_CI} = \frac{\text{FWI}_{\text{max}} - \text{FWI}}{\text{FWI}_{\text{max}} - \text{FWI}_{\text{min}}} \quad (8)$$

This new index assesses the value of FWI compared to the extreme values for the specific region since values of the FWI alone can have a different interpretation for different ecosystems. According to the equation describing the FWI_CI, values of the index close to 1 will be the result of low FWI tending towards the FWI_{min} values, with the opposite being true for values close to 0.

In order to compose and study the effectiveness of the newly formed index, a total of 67 points were selected in GEE, for which the required indices were calculated. Reflectance and LST data for the calculation of the VCI and TCI were obtained by the COPERNICUS/S2_SR_HARMONIZED and MODIS/061/MOD11A products. Data for the calculation of the FWI_CI was received from the CFSR dataset.

For the calculation of the new index, FWI_{veg}, a genetic algorithms approach was implemented aiming to acquire algorithms that optimally reflect fire danger by combining the two indices. The structure of these algorithms consists of mathematical expressions displayed in Table 1 that combine the FWI_CI and VHI based on certain logical conditions (OR/AND) as well as thresholds regarding their values.

Each produced algorithm is defined by its “gene”, which bears information about which conditions and mathematical expressions were used to compose the algorithm. Genes of algorithms are combined in pairs to produce new algorithms that inherit some attributes (conditions and expressions) from each one of their two parent algorithms.

Prior to pair-crossing algorithms to create offspring, each algorithm was assessed on its fitness. Before calculating the fitness function, the percentage of detected ignitions was calculated for the values of the index that were lower than the 10th, 30th, 50th, 70th and 90th percentile. As mentioned above, the magnitude of the values of the component indices (FWI_CI, VHI) is disproportional to fire danger. The Mann–Kendall test [64] was performed for each algorithm with the purpose of detecting the existence of a trend between the index percentile values and the percentages of detected ignitions.

Thus, the fitness of each produced algorithm was assessed based on the existence (or not) of a trend and, in a second phase, the absolute slope, with both metrics provided by the Mann–Kendall test. The aim was to find algorithms that presented a trend regarding fire danger as well as a steep slope (>75th percentile) indicating significant changes in fire danger with respect to the values of the index.

Table 1. Joint functions, conditions and mathematical expressions for the construction of algorithms. Notations x, y refer to the indices FWI_CI, VHI accordingly. Two or more mathematical expressions are used to construct potential algorithms for the new index. These mathematical expressions are selected based on the conditions in the middle column that can potentially be combined through the Joint functions of the left column.

Joint Functions	Conditions	Mathematical Expressions
OR	$x - y > 0.7$	$0.4 \times x + 0.6 \times y$
AND	$x < 0.5$	$0 \times (x + y)$
	$y < 0.5$	$0.5 \times (x + y)$
	$y - x < 0.5$	$0.7 \times x + 0.3 \times y$
		$0.8 \times x + 0.2 \times y$
		$e^x + y$
		$e^y + x$
		$x^2 + y$
		$y^2 + x$
		$x^2 + y^2$
		$\sqrt{x^2 + y^2}$

Initially, a total of 102 algorithm genes were created as population zero, and the entire process was run in a repetitive fashion using a loop for a total of 5 generations.

2.7. Validation—The Fire in Mati as a Pilot Case Study

The components of the FWIveg index were used for fire prediction in the case of Mati wildfire in the region of Attica (23 July 2018). The fire is considered one of the most destructive wildfire incidents in Greece [65]. The Mati fire happened simultaneously with the fire in Kinetta, leading to a total burned area of 14.48 km² and 102 victims [65]. The meteorological conditions of the region (Temperature (T) > 40 °C, Relative Humidity (RH) \cong 19% and Wind speed (Ws) up to 34.4 m/s) during the ignition day greatly assisted the propagation of the fire front, whose propagation was stopped in the coastline of the region [65].

Information for a total of seven fire incidents in Greece was collected in order to compose the VHI and FWI_CI. Information for the calculation of the VHI came from the COPERNICUS/S2_SR_HARMONIZED dataset of the European Copernicus database and the MODIS/061/MOD11A1. The FWI_CI was calculated using data coming from the meteorological station network of the Greek observatory of Athens (<https://meteosearch.meteo.gr/data/index.cfm> (accessed on 10 October 2022)). Fire incidents are presented in Table 2.

Table 2. Selected fire locations for validation purposes.

Location	Date
Kinneta	23 July 2018
Istiaia	10 August 2021
Agios Stefanos	6 August 2021
Palaiokoundoura Mandras	20 May 2021
Styra	8 August 2021
Psaxna	13 August 2019
Mati	23 July 2018

All indices were calculated for a span of 6 days, covering the ignition date and the previous 5 days. The indices VCI and TCI were calculated for a span of 10 days, including the ignition day, since the Sentinel 2 satellite system has a temporal coverage of 5 days. To obtain the intermediate values of the interested 6-day period, interpolation was performed, and the values were calculated based on the equation of the tendency of the indices for the 10-day period.

The VHI was calculated in GEE, while the FWI_CI was calculated in C++ programming language by a program specifically designed for short-term calculations of the index.

What followed was the composition and training of a different ANN in python language that used the VHI and FWI_CI values of all incidents except that of Mati for their respective six-day periods as input. The network was trained with a learning rate of 0.1, and the number of epochs was set to 10,000. In order to find the fire incident that most accurately resembles the conditions (FWI_CI, VHI) of the Mati fire 5 days prior to ignition, the cumulative difference of the values of the indices was calculated between each incident and that of *Mati* for the span of the 5 days, as shown in Equation (9).

$$\begin{aligned} \text{Difference}(\text{fire incident}) & \left| \sum_{i=0}^{i=5} \text{FWI}_{CI}(\text{fire incident}) - \sum_{i=0}^{i=5} \text{FWI}_{CI}(\text{Mati}) \right| \\ & + \left| \sum_{i=0}^{i=5} \text{VHI}(\text{fire incident}) - \sum_{i=0}^{i=5} \text{VHI}(\text{Mati}) \right| \end{aligned} \quad (9)$$

In Equation (9), the difference is calculated as the addition of the cumulative difference of the two indices between the Mati region and all other locations for the 5 days prior to ignition. The best-matching fire incidents were chosen to be the ones whose difference was below the 25th percentile of all differences corresponding to the six locations. Those locations were found to be “Agios Stefanos” and “Psaxna”. Hence, the network was trained based on the FWI_CI and VHI profiles of these regions during the six-day periods.

Predictions received a value of 0 or 1 corresponding to the states of “no ignition” or “ignition” accordingly. The network was initiated 4 times, and the mean state of predictions was taken into account (Figure 3).

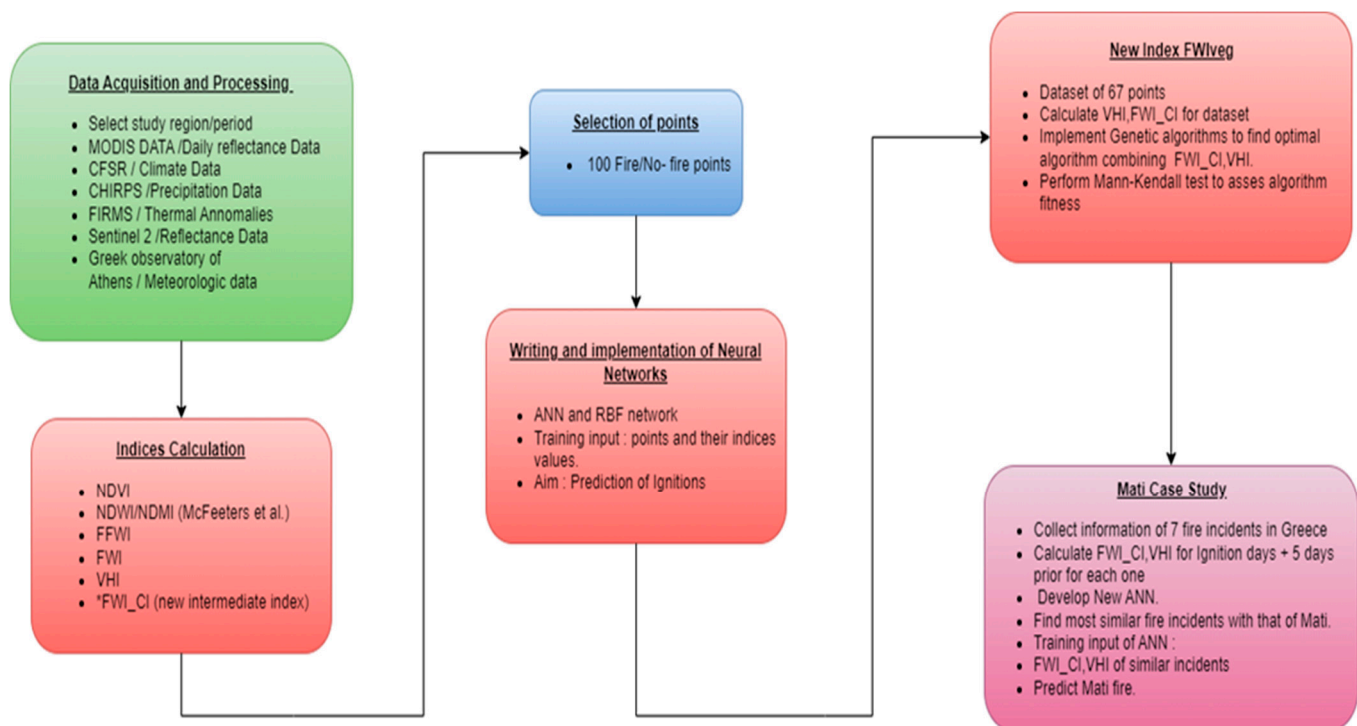


Figure 3. Schematic representation of methodology procedures through a flow chart. Each box of the figure represents a stage of the methodology through brief steps. Although the final stage of the Mati case study can be performed independently from the rest of the methodology, the former was necessary for its conceptualization as well as assessment of results.

3. Results

In this section, the results of Section 2 are presented and discussed in detail. The results of index calculations in GEE are graphically represented in Figure 4, with statistics about the indices shown in Table 3. In general, both neural networks had sufficient performance

regarding ignition prediction. Through consecutive generations, the obtained algorithm for the new index, FWIveg, presented sufficient correlation with the number of ignitions per point, while the neural network implemented for the Mati pilot case study was able to accurately predict ignition-deriving information from the FWIveg.

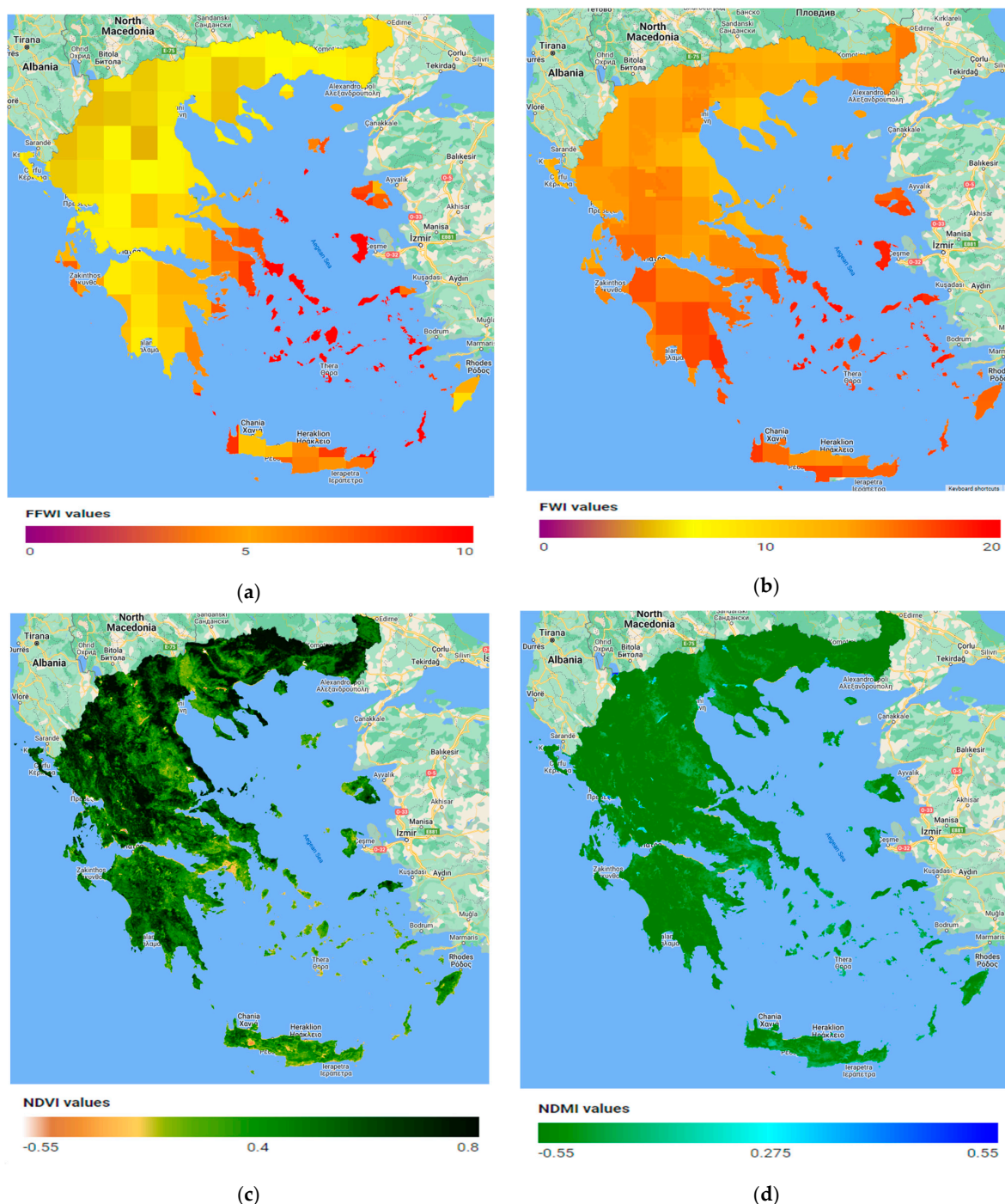


Figure 4. Representation of the indices calculated in GEE to be used as input values for the neural networks for the study region of Greece, FFWI (a), FWI (b), NDVI (c), NDMI (d). The indices FWI, FFWI present a similar spatial distribution pattern, concentrating their higher values on the hot and dry south-eastern part of the country. NDVI and NDMI values have been limited within the range displayed in the legends to better depict contrast and value variations within the study region.

Table 3. Statistics for the minimum, median, maximum and percentile values of the input indices calculated in GEE. Rows correspond to the median values of the indices for the study region throughout the study period, whereas columns refer to the respective values of each index series for the 100 selected points.

	Count	Min	Mean	Max	25th Percentile	50th Percentile	75th Percentile
FWI median	100	10.289	11.246	11.049	11.252	11.455	11.951
FFWI median	100	4.955	4.095	4.563	4.829	5.125	6.219
NDVI median	100	0.154	0.423	0.728	0.318	0.420	0.522
NDMI median	100	−0.976	−0.468	−0.380	−0.533	−0.476	−0.409
Ignitions	100	0	0	0	0	1	5

3.1. ANN Results

The T_{MAE} was proven to exhibit a linear dependence on the epoch number with a proportional increasing trend, with an $R^2 = 0.99$, $p < 0.05$ and a slope of 1.04 (Figure 5b). The values of the T_{MAE} for the epoch numbers (100, 500, 1000, 5000, 10,000, 25,000) were 9, 53, 109, 553, 1009 and 2775 epochs, respectively.

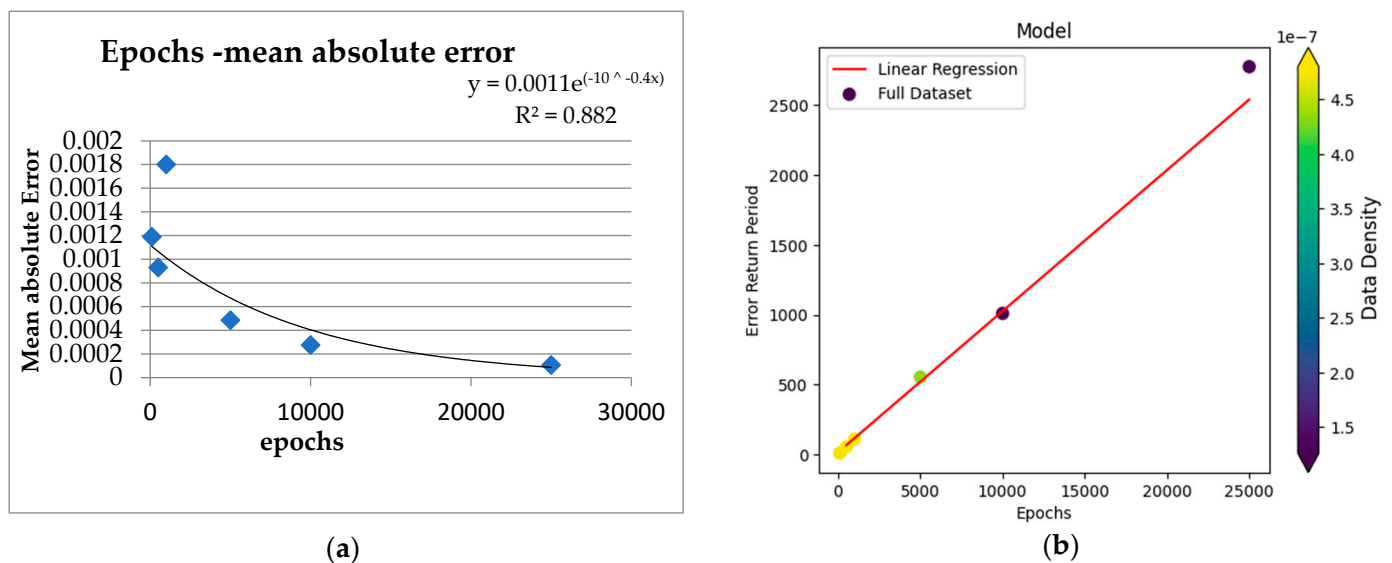


Figure 5. Correlation of MAE–epoch number (a). Correlation of T_{MAE} –epoch number (b). Increased number of epochs during the training phase leads to a lower MAE as well as a higher return period of MAE > 0.25 (T_{MAE}).

The MAE at the end of each training process for each epoch number was also used to act as a choice criterion for the optimal number of epochs. The equation portraying the relationship between the number of epochs and the final MAE is given by equation $y = 0.0011e^{(-10^{-0.4x})}$, $R^2 = 0.882$ and is displayed in Figure 5a. Both the negative notation on the exponent and the chart revealed the decreasing trend of the final MAE as the number of epochs increased.

Despite improvements in ANN efficiency with the increase in epoch numbers that can be seen in the increase of T_{MAE} , as well as the decrease in the final value of the MAE during training, the latter was already negligible for 500 epochs. In the case of the current study, 10,000 epochs were selected for the ANN training. This number maximizes accuracy by reducing error; after 10,000 epochs, calculations start to become time intensive without any notable increase in accuracy.

After predictions were made for the 10th test batch by applying parameters of all nine trained batches, the Cumulative Absolute Error (CAE) was calculated for the total number of points (10) in the batches. The best-performing batch by that metric was found to be the fourth (row index 3 in Table 4), corresponding to points 30–40 of the 90-point shuffled training dataset. Apart from the similarities in CAE portrayed in Table 4, the fourth batch produced the most similar ignition curve displayed in Figure 6, which represents the exact number of ignitions per point.

Table 4. Cumulative Absolute Error (CAE) and total numbers of predicted and actual ignitions based on predictions from the parameters of the various train batches. The CAE is the summation of the MAE for the ten points of the test batch.

Training Batch	CAE	Tot. Predicted Ignitions	Tot. Actual Ignitions	Absolute Difference
0	1.238	8	8	0
1	1.766	10	8	2
2	1.471	8	8	0
3	0.948	6	8	2
4	1.206	6	8	2
5	1.319	10	8	2
6	0.962	7	8	1
7	1.672	6	8	2
8	1.243	17	8	11

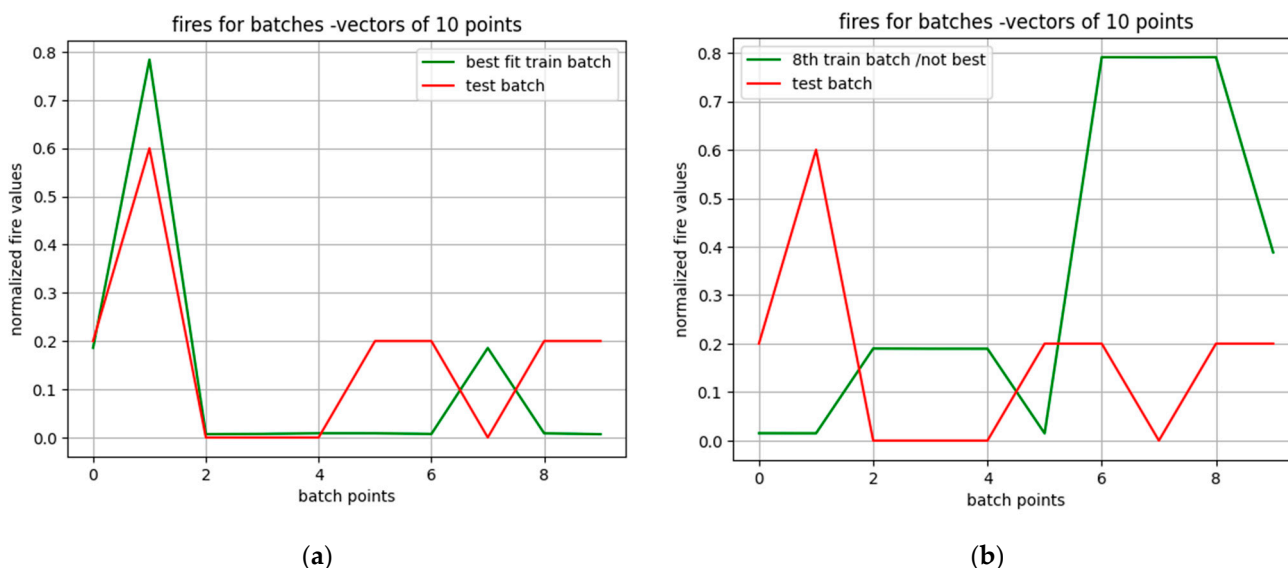


Figure 6. Comparison of similarity of ignition curves, meaning actual number of ignitions (red line) and predicted number of ignitions (green line), with the predicted one from the parameters of the corresponding train batch. Chart (a) depicts predictions made using the parameters (w,b) of the 4th optimal batch, while chart (b) corresponds to predictions made using parameters of a non-optimal batch (8th). The y-axis corresponds to the number of ignitions Y after being divided by its maximum value (5); hence, to obtain the true ignitions for each point, the y-values of the curves have to be multiplied by 5.

3.2. RBF Results

According to the error matrix discussed in Section 2, the training batch whose parameters achieved the most accurate predictions regarding the actual state of the fifth test

batch was the second training batch, for which the MAE was roughly 0.0077, two orders of magnitude below errors produced by other batches.

$$MAE \text{ Matrix} = \begin{bmatrix} 0.5004435 \\ 0.0077347 \\ 0.6963062 \\ 0.5008662 \end{bmatrix} \quad (10)$$

Table 5 presents the total number of predicted and actual ignitions based on different prediction scenarios for both types of neural networks.

Table 5. Total number of predicted and actual ignitions based on predictions using parameters of the various training batches for both types of neural networks.

Row Index	Predictions RBF (2nd Batch)	Actual Ignitions	Predictions ANN (4th Batch)	Actual Ignitions	Absolute Difference RBF, ANN
0	1	1	1	1	[0, 0]
1	1	1	4	3	[0, 1]
2	0	0	0	0	[0, 0]
3	1	0	0	0	[1, 0]
4	0	1	0	0	[1, 0]
5	0	0	0	1	[0, 1]
6	0	0	0	1	[0, 1]
7	1	1	1	0	[0, 1]
8	1	1	0	1	[0, 1]
9	1	1	0	1	[0, 1]
Summary	6	6	6	8	

3.3. Results of the ROC Method

According to Table 5, ROC metrics for the results produced by the RBF network were TP = 5, FP = 1, TN = 3 and FN = 1, while the same terms for the ANN were TP = 2, FP = 1, TN = 3 and FN = 4. The terms TPR and FPR were 0.833 and 0.1818 for the RBF network, as well as 0.667 and 0.1818 for the ANN. Judging by the aforementioned metrics, the RBF network presented higher accuracy compared to the ANN, with the same being true for the total number of predicted ignitions. However, the correct prediction of 66.67% of ignitions in a region could be satisfactory as far as concerns the estimation of fire danger. An additional important metric is the ratio of FPR/TPR. When the ratio approaches the value of 1, signifying near equal FPR and TPR terms, there is a 50% chance that the network predicts an ignition either correctly or incorrectly. Thus, the ratio is required to be as close to zero as possible. The ratio for the ANN network was 0.272, well below the threshold of 1, while for the RBF network, the same term was 0.218. Table 6 displays statistics of the ROC method for both neural networks.

Table 6. Assessment indices of the (ROC) method for both networks.

	RBF	ANN
TP	5	2
FP	1	1
TN	3	3
FN	1	4
TPR%	83.33	66.67
FPR%	18.18	18.18
FPR/TPR	0.218	0.272

Another criterion could be used for the accuracy assessment of the ANN, such as when the total number of predicted ignitions accuracy reaches 75%. If instead of the exact number

of ignitions of each point, the aim was the prediction of the total number of ignitions for the total of 10 points (that could potentially define an arbitrary region of the study area), prediction accuracy, in this case, can reach up to 87.5% by taking into account results from predictions of the sixth batch in Table 4.

3.4. Results of the Vegetation-Enhanced FWI (FWIveg)

Concerning the FWIveg, the results of the Mann–Kendall test revealed the general evolution of the algorithm population towards a state that better describes fire danger. Between the initial population and that of the final fifth generation, the mean slope of the Mann–Kendall test presented an increase in its absolute value of 21.53%. The τ variable increased by 17.35%, while the z-core and p -values increased their absolute values by 17.74% and 84.56%, respectively. All values except the p -value were negative, indicating a decreasing trend, which revealed increased fire danger as index values decreased and vice versa. The initial mean p -value was 0.116 and dropped to 0.0179 during the fifth generation, presenting a decrease of an order of magnitude. The term “trend” of the Mann–Kendall test received a value of 1 when the test detected a trend and 0 for the absence of it. Its mean value increased by 18.6%, reaching 1, indicating the presence of a trend in all algorithms. The total algorithm population of the fifth generation was 4. Specifically, the generation population presented a decrease from 102 (initial population generation 0) to 23, 9, 4, 4 and 4 for the five consecutive generations. Results of the evolution process as well as the produced algorithms, are presented in greater detail in Table 7 and Appendix A.

Table 7. Variation of Mann–Kendall variables over the span of 5 generations of produced algorithms.

Generations	Slope	Trend	τ	z-Score	p -Value	S
0	−4.712	0.843	−0.710	−2.187	0.116	−14.9
1	−5.685	1	−0.801	−2.405	0.020	−16.8
2	−5.905	1	−0.762	−2.279	0.024	−16.0
3	−5.72	1	−0.833	−2.507	0.018	−17.5
4	−5.85	1	−0.786	−2.355	0.027	−16.5
5	−5.72	1	−0.833	−2.507	0.018	−17.5

Table 8 displays the final algorithm of the fifth generation. The algorithm is written in pseudo-code, with x referring to the initial value of the FWI_CI and x' to the new value of the x after the mathematical expressions of Section 2 have been applied. The same goes for the value y , referring to the initial value of the VHI. The term Z in the end, refers to the new index FWIveg.

Table 8. Algorithm 4 of generation 5 for the calculation of FWIveg. Values x , y , Z represent the FWI_CI, VHI, FWIveg.

Algorithm 4 Generation 5	
1.	If $x < 0.5$ OR $y < 0.5$:
2.	$x' = x^2$
3.	$y' = y$
4.	Else:
5.	$x' = 0.5 \times x$
6.	$y' = 0.5 \times y$
7.	$Z = x' + y'$

3.5. Validation of Results—The Fire in Mati as a Pilot Case Study

Predicted values for the Mati case ranged in the neighborhood of 0 for the 5 days prior, with a value of 0.999925 (essentially 1) being predicted for the sixth day of the ignition (Table 9).

Table 9. Predicted (mean values of 4 runs) for the six-day period regarding the Mati case, alongside daily probabilities of ignition, as calculated by Equation (11), versus the actual state for the Mati fire.

Date	Predicted State	Probability of Ignition	Actual State
18 July 2018	0.0	0.0	0
19 July 2018	0.0	0.0	0
20 July 2018	2×10^{-193}	2×10^{-193}	0
21 July 2018	1.1×10^{-295}	1.1×10^{-295}	0
22 July 2018	0.0	0.0	0
23 July 2018	0.999925	1	1

Being aware that the ignition happened on the sixth day (23 July 2018), it can be claimed that the network performed an accurate prediction that highly resembles the actual state. To achieve a better interpretation of the predicted results, the probability of ignition was calculated as the value of each day's prediction divided by the summary of the values of all six predictions, according to Equation (11). The near-zero and zero values for the five days prior to ignition mean near-zero ignition probabilities, with the probability of the sixth day for which the ignition occurs receiving a value of 1.

$$y_{\text{predicted_new}_i} = \frac{y_{\text{predicted}_i}}{\sum_{n=0}^i y_{\text{predicted}_n}} \quad (11)$$

4. Discussion

The results of the predicted ignitions by neural networks are considered satisfactory, being able to achieve TPR of 66.67% (ANN) and 83.33% (RBF), as well as TPR/FPR ratios of 0.272 and 0.218 accordingly. Accuracy for the ANN can reach up to 87.5% if only the total number of predicted/actual ignitions is used as the sole criterion, and thus parameters of the seventh batch (index 6 in Table 4) were used for predictions. The T_{MAE} was found to be linearly dependent on the number of epochs $R^2 = 0.99$, $p < 0.05$, while the dependence of the final MAE value itself was found to be exponential, exhibiting an inverse relationship. The optimal number of epochs was deemed to be 10,000 for the ANN, with very low MAE values (0.00119–0.000106) yielded even for 1000 epochs.

The only limitation regarding epoch numbers for the ANN was the computational intensity and time demand of calculations for numbers of epochs going past 10,000. Further, increasing the number of epochs did not contribute to a substantial improvement in the accuracy of the predicted results; hence, 10,000 was selected for the training phase of the ANN. For the RBF network, predictions using the parameters of the second batch were found to be the most accurate.

Calculation of the newly developed index, the FWIveg, through the genetic algorithms approach, yielded useful results. After five generations of algorithms, the FWIveg index was able to perform a gradual classification of fire danger. Points with low index values accumulated high numbers of ignitions; in addition, the results of the Mann–Kendall test revealed a decreasing trend regarding index values and percentage of ignitions, thus reinforcing the above claim.

A new ANN was developed and tasked with predicting the Mati wildfire incident (23 July 2018), taking as input the two components of the FWIveg. After assessing fire incident similarity based on the difference of said components, the network was trained by receiving as input values the two component indices (VHI, FWI_CI) of the optimal incidents for a depth of 6 days (ignition day + 5 days prior). After identifying the optimal fire incidents (“Agios Stefanos”, “Psaxna”) that best simulate the Mati case, it predicted the fire of Mati using the optimal W,B parameters derived from the training process with an ignition probability of 100%.

In a similar context, Edwards et al. [66] managed to achieve an accuracy of 78.73% by proposing a new, improved accuracy method, named “balanced accuracy”, regarding

ignition prediction for the region of Madagascar. Al-Kahlout et al. [67] used the “Just Neural Network (JNN)” approach, together with the FWI, in order to predict burnt area for the region of Portugal with an accuracy of 99.98%. Wu et al. [68] managed to predict wildfires using neural networks with meteorological variables as input, as well as vegetation input and topography features for the region of Heilongjiang, China, achieving an F-measure accuracy [68] of up to 95.26%. In the study of Caraballo et al. [51], an accuracy of 75.8/76%, and an MSE of 0.23–0.24, were reached using ANN for predicting ignition/no-ignition state based on the values of the FWI and its subcodes.

The enrichment of the FWI has already been performed with additional vegetation or meteorological indices to expand its results upon different aspects relating to wildfires. In the case of Pinto et al. [69], the index was enriched with the Continuous Haines Index (CHI) in order to more accurately predict energy release during wildfires as an index of their intensity. The NDVI index can be used as a metric of drought-related vegetation stress of a region, whereas it can also be used to assess the productivity of a region and, thus, provide information about fuel availability, structure and attributes closely related to the phenomenon of wildfires [70].

Gabban et al. [71] compared the FWI and NDVI regarding their ability to optimally express fire danger in a region based on fire incident accumulation. It was proven that the FWI performs better in association with NDVI. According to the study of Bugalho et al. [72], an estimated 88% of high-intensity fires, meaning those that lead to a burned area >1000 ha, occur in regions that are covered >20% by non-healthy vegetation (VHI < 40%) [71]. According to Chéret et al. [73], there is an indirect correlation between the proxy indices of the NDVI and wildfires. Such proxy indices include the Spring Greenness Index (SG) and the Relative Greenness Index (RGRE), which assess fuel production and seasonality of the NDVI, with the importance of the latter in wildfires also having been highlighted in the study of Talucci et al. [74]. Talucci et al. [74] used a classification model for fire danger based on values of the FWI, NDVI and δ NDMI. It was proven that the FWI was the most influential index, with the NDVI being the second most influential regarding fire danger by assessing vegetation state before ignition. Additional information stemming from the NDVI is the attribute of phytophysiognomy, which has been proven to be correlated to the seasonality of wildfires. Finally, the NDVI and NDMI have been used by Abdollahi et al. [75] in order to classify fire danger in Alberta, Canada, being able to correctly predict 77% of recorded wildfires in the region.

The optimal algorithm that was produced for the calculation of the new index (FWIveg) (Table 8) demonstrates that FWI_CI values have a higher influence on final index values compared to the VHI, which is an NDVI proxy when they are below the 0.5 threshold. The VHI is a proxy index of NDVI-assisted fire prediction for the case of Mati, while the NDVI itself was also able to adequately achieve fire prediction regarding the 100 selected points. Phytophysiognomy, as well as the amount of fuel production, are dependent not only on the mean NDVI values but also on the difference between minimum and maximum values during the annual cycle, demonstrating plant development patterns over the year, which correlates to biomass, and hence, fuel production [69]. This is the reason minimum and maximum values of the index were also taken into account in Section 2. The above characteristics can play an important role in fire prediction by functioning as proxy metrics of vegetation characteristics since, according to Leblon et al. [76], the correlation of NDVI and FWI is species dependent.

It has been highlighted that the inclusion of the NDVI itself, as well as proxy indices, can reveal critical information about vegetation that greatly amplifies and improves the results of the FWI. Implementing neural networks for that purpose can be a much more effective solution than separately studying the results of each index.

Limitations of the current study stemmed from the computational power of the GEE and the study region’s complex geometry, necessitating temporal segmentation of all calculation procedures. The spatial resolution of the CFSR dataset (38 km) was much coarser than that of the MOD09GA.061 (500 m). A higher performance could be achieved

for all neural networks with a higher volume of input data. Using randomly selected points for the calculation also leads to a loss of information about the intermediate region. Under the current framework, future work will direct effort in the writing of neural networks on the GEE environment itself, while also attempting to find a correlation between remotely-sensed indices and the FWI in order to conduct the entire study on GEE, eliminating the loss of information coming from studying distinct points.

5. Conclusions

The conjunction of fire and vegetation indices can produce useful information regarding fire favorability due to meteorology and fuel properties in order to perform accurate fire danger classification. The specific (local) information we need is directly or indirectly related to the expected number of ignitions or their expected intensity and consequences. However, the increased complexity characterizing the links and relationships between the various mechanisms related to wildfires, in conjunction with the stochasticity of the phenomenon, leads us to the conclusion that indices' values are not directly related to ignitions.

The previously mentioned reasons, combined with the high volume of data, either favor or necessitate the implementation of neural networks. In the current study, two fire indices (FWI, FFWI) and two remotely sensed indices (NDVI, NDMI) were used as inputs for two categories of neural networks (ANN, RBF) in order to predict ignitions in a random set of 100 points. A new index (FWIveg) was composed, combining indirect information from the FWI and VHI. The methodology of genetic algorithms was used to calculate the index in order to better classify fire danger.

The two neural networks used on the dataset of 100 points achieved a TPR-based accuracy of TPR = 83.33% and 66.67% for the RBF and ANN, respectively, with accuracy reaching as high as 87.5%, when accuracy was measured as the ratio of predicted/actual ignitions. The new index FWIveg performed satisfactorily in classifying gradual fire danger. Using components of the FWIveg, the new ANN was able to accurately predict ignition on the sixth day (23 July 2018), with an achieved probability of ignition of 100%.

All neural networks achieved better performance and higher accuracy, with the ability to perform training with a higher volume of data (more points), as well as more continuous data by processing satellite images directly from GEE instead of discrete points. Such drawbacks will be tackled by aiming to compose and implement neural networks directly on GEE in future studies. In order to apply the methodology to a continuous spatial domain, we will be deriving information from multiband satellite images. The new proposed index could be further investigated by performing applications of it on different study regions and ecosystems in order to acquire a link between fire danger as described by index values and vegetation-specific attributes such as structure, density as well as growth and development patterns throughout the annual cycle. The new index could also serve the purpose of providing a quantitative metric about the attribution of fire danger, thus separating between 'vegetation-based fire danger', 'meteorology-based fire danger' and 'equal fire danger' when both meteorology and vegetation of a region present a near-equivalent contribution to fire danger.

Other types of algorithms and methods are also aimed to be explored and implemented in future efforts by aiming to adapt their application in order to yield fire-related results. Firework-type algorithm approaches can be a promising methodology since they are able to perform large-scale blackbox optimization and complex searches, such as the example of Chen et al. [77], who proposed a novel Self-Adaptive Fast Fireworks algorithm (SF-FWA). Certain algorithms that are based on the concept of polypleidy, such as in the case of Maxim et al. [78], could further enhance research efforts and results in the domain of fire danger by being able to construct much more complex algorithms that more accurately calculate fire danger. Algorithms that are used for routing, or production chain optimization, such as the ones examined in the study of Pasha et al. [79] and Gholizadeh et al. [80], could play a crucial role in fire suppression planning and efficient resource

allocation based on fire danger as well as various other fire related factors. Maxim et al. [81] used a Diffused Memetic Optimizer (DMO) for berth allocation during disruptive events. Such approaches could play a crucial role in mitigation strategies during and after the incidence of a wildfire by optimizing population evacuation, hospitalization as well as post-fire allocation procedures. Ant algorithms could be a promising approach towards the problem of algorithm generation for fire danger. Following this approach, individual algorithms could explore the “algorithm space” and exchange information with one another independently and simultaneously, mimicking the way ants explore a spatial domain exchanging information through pheromone release [82,83].

Implementation of such advanced methods could increase the accuracy of results by producing algorithms of higher complexity that better describe fire danger, as well as being able to process higher volumes of input data.

Author Contributions: Conceptualization, N.N.; data curation, N.N.; formal analysis, N.N.; investigation, N.N.; methodology, N.N.; project administration, S.S., O.C. and A.S.; resources, N.N.; software, N.N.; supervision, S.S., O.C. and A.S.; validation, N.N.; visualization, N.N.; writing—original draft, N.N.; writing—review and editing, N.N. and S.S. All authors have read and agreed to the published version of the manuscript.

Funding: This research received no external funding.

Institutional Review Board Statement: Not applicable.

Informed Consent Statement: Informed consent was obtained from all subjects involved in the study.

Data Availability Statement: Data for the calculation of remote sensing indices was acquired from the COPERNICUS/S2_SR_HARMONIZED product of GEE (https://developers.google.com/earth-engine/datasets/catalog/COPERNICUS_S2_SR_HARMONIZED), as well as the MOD09GA.061 (https://developers.google.com/earth-engine/datasets/catalog/MODIS_061_MOD09GA), product, (both accessed on 7 March 2023). Meteorological Data for the calculation of the FWI and FFWD came from the CFSR (https://developers.google.com/earth-engine/datasets/catalog/NOAA_CFSR) and CHIRPS (https://developers.google.com/earth-engine/datasets/catalog/UCSCHG_CHIRPS_DAILY), datasets accessed on 7 March 2023. Data for the monitoring of wildfires came from the FIRMS dataset (<https://www.earthdata.nasa.gov/learn/find-data/near-real-time/firms>) accessed on 7 March 2023. The LST was obtained from the MODIS/061/MOD11A GEE product of Modis (https://developers.google.com/earth-engine/datasets/catalog/MODIS_061_MOD11A1) accessed on 7 March 2023. The Mati station data for the calculation of the FWI came from the Greek observatory of Athens (<https://meteosearch.meteo.gr/data/index.cfm>) (accessed on 7 March 2023).

Acknowledgments: A part of this paper is a section of the masters’ thesis submitted as partial fulfillment of the Master of Science in Sustainable Management of Environmental Change and Cyclical Economy.

Conflicts of Interest: The authors declare no conflict of interest.

Appendix A

In the current section, generated algorithms are displayed in Tables A1–A5. The algorithms correspond to 1 randomly selected algorithm of generation 1 and the 4 final algorithms of generation 5.

Table A1. Algorithm 1 of generation 1 for the calculation of FWIveg. Values x , y , Z represent the FWI_CI, VHI, FWIveg.

Algorithm 1 Generation 1	
1.	If $x - y > 0.7$:
2.	$x' = x$
3.	$y' = e^y$
4.	Else if $y - x > 0.7$ AND $x < 0.5$:
5.	$x' = x^2$
6.	$y' = y^2$
7.	Else:
8.	$x' = e^x$
9.	$y' = y$
10.	$Z = x' + y'$

Table A2. Algorithm 1 of generation 5 for the calculation of FWIveg. Values x , y , Z represent the FWI_CI, VHI, FWIveg.

Algorithm 1 Generation 5	
1.	If $y - x > 0.7$:
2.	$x' = 0.5 \times x$
3.	$y' = 0.5 \times y$
4.	Else if $y - x > 0.7$ OR $y < 0.5$:
5.	$x' = x^2$
6.	$y' = y$
7.	Else:
8.	$x' = x^2$
9.	$y' = y^2$
10.	$Z = x' + y'$

Table A3. Algorithm 2 of generation 5 for the calculation of FWIveg. Values x , y , Z represent the FWI_CI, VHI, FWIveg.

Algorithm 2 Generation 5	
1.	If $x - y > 0.7$:
2.	$x' = x^2$
3.	$y' = y^2$
4.	Else if $x < 0.5$ AND $y < 0.5$:
5.	$x' = x$
6.	$y' = y^2$
7.	Else:
8.	$x' = 0.5 \times x$
9.	$y' = 0.5 \times y$
10.	$Z = x' + y'$

Table A4. Algorithm 3 of generation 5 for the calculation of FWIveg. Values x , y , Z represent the FWI_CI, VHI, FWIveg.

Algorithm 3 Generation 5	
1.	If $x < 0.5$ AND $y < 0.5$:
2.	$x' = x^2$
3.	$y' = y^2$
4.	Else:
5.	$x' = x^2$
6.	$y' = y^2$
7.	$Z = x' + y'$

Table A5. Algorithm 4 of generation 5 for the calculation of FWIveg. Values x, y, Z represent the FWI_CI, VHI, FWIveg.

Algorithm 4 Generation 5	
1.	If $x < 0.5$ OR $y < 0.5$:
2.	$x' = x^2$
3.	$y' = y$
4.	Else:
5.	$x' = 0.5 \times x$
6.	$y' = 0.5 y$
7.	$Z = x' + y'$

References

- Tavakkoli Piralilou, S.; Einali, G.; Ghorbanzadeh, O.; Nachappa, T.G.; Gholamnia, K.; Blaschke, T.; Ghamisi, P. A Google Earth Engine Approach for Wildfire Susceptibility Prediction Fusion with Remote Sensing Data of Different Spatial Resolutions. *Remote Sens.* **2022**, *14*, 672. [\[CrossRef\]](#)
- Ghorbanzadeh, O.; Blaschke, T.; Gholamnia, K.; Aryal, J. Forest Fire Susceptibility and Risk Mapping Using Social/Infrastructural Vulnerability and Environmental Variables. *Fire* **2019**, *2*, 50. [\[CrossRef\]](#)
- Lü, A.; Tian, H.; Liu, M.; Liu, J.; Melillo, J.M. Spatial and Temporal Patterns of Carbon Emissions from Forest Fires in China from 1950 to 2000. *J. Geophys. Res. Atmos.* **2006**, *111*, D05313. [\[CrossRef\]](#)
- Moayedi, H.; Mehrabi, M.; Bui, D.T.; Pradhan, B.; Foong, L.K. Fuzzy-Metaheuristic Ensembles for Spatial Assessment of Forest Fire Susceptibility. *J. Environ. Manag.* **2020**, *260*, 109867. [\[CrossRef\]](#)
- Sayad, Y.O.; Mousannif, H.; Al Moatassime, H. Predictive Modeling of Wildfires: A New Dataset and Machine Learning Approach. *Fire Saf. J.* **2019**, *104*, 130–146. [\[CrossRef\]](#)
- Boer, M.M.; Nolan, R.H.; Resco De Dios, V.; Clarke, H.; Price, O.F.; Bradstock, R.A. Changing Weather Extremes Call for Early Warning of Potential for Catastrophic Fire. *Earth's Future* **2017**, *5*, 1196–1202. [\[CrossRef\]](#)
- Haynes, K.; Short, K.; Xanthopoulos, G.; Viegas, D.; Ribeiro, L.M.; Blanchi, R. Wildfires and WUI Fire Fatalities. In *Encyclopedia of Wildfires and Wildland-Urban Interface (WUI) Fires*; Manzello, S.L., Ed.; Springer: Cham, Switzerland, 2020; pp. 1–16. [\[CrossRef\]](#)
- Sfougaris, A.; Plexida, S.; Solomou, A. Assessing the Effects of Environmental Factors on the Presence and Density of Three Shrike Species in a Continental and a Coastal Area of Central Greece. *North-West. J. Zool.* **2014**, *10*, 101–109.
- Sulova, A.; Jokar Arsanjani, J. Exploratory Analysis of Driving Force of Wildfires in Australia: An Application of Machine Learning within Google Earth Engine. *Remote Sens.* **2021**, *13*, 10. [\[CrossRef\]](#)
- Vardoulakis, S.; Marks, G.; Abramson, M.J. Lessons Learned from the Australian Bushfires: Climate Change, Air Pollution, and Public Health. *JAMA Intern. Med.* **2020**, *180*, 635–636. [\[CrossRef\]](#)
- Wang, X.; Thompson, D.K.; Marshall, G.A.; Tymstra, C.; Carr, R.J.; Flannigan, M.D. Increasing Frequency of Extreme Fire Weather in Canada with Climate Change. *Clim. Chang.* **2015**, *130*, 573–586. [\[CrossRef\]](#)
- Abatzoglou, J.; Kolden, C. Relationships between Climate and Macroscale Area Burned in the Western United States. *Int. J. Wildland Fire* **2013**, *22*, 1003. [\[CrossRef\]](#)
- Vasiliades, L.; Loukas, A. Hydrological Response to Meteorological Drought Using the Palmer Drought Indices in Thessaly, Greece. *Desalination* **2009**, *237*, 3–21. [\[CrossRef\]](#)
- Sakellariou, S.; Sfougaris, A.; Christopoulou, O.; Tampekis, S. Integrated Wildfire Risk Assessment of Natural and Anthropogenic Ecosystems Based on Simulation Modeling and Remotely Sensed Data Fusion. *Int. J. Disaster Risk Reduct.* **2022**, *78*, 103129. [\[CrossRef\]](#)
- Sakellariou, S.; Sfougaris, A.; Christopoulou, O.; Tampekis, S. Spatial Resilience to Wildfires through the Optimal Deployment of Firefighting Resources: Impact of Topography on Initial Attack Effectiveness. *Int. J. Disaster Risk Sci.* **2023**, *14*, 98–112. [\[CrossRef\]](#)
- Resco de Dios, V.; Cunill Camprubí, À.; Pérez-Zanón, N.; Peña, J.C.; Martínez del Castillo, E.; Rodrigues, M.; Yao, Y.; Yebra, M.; Vega-García, C.; Boer, M.M. Convergence in Critical Fuel Moisture and Fire Weather Thresholds Associated with Fire Activity in the Pyroregions of Mediterranean Europe. *Sci. Total Environ.* **2022**, *806*, 151462. [\[CrossRef\]](#)
- Leidner, A.K.; Buchanan, G.M. (Eds.) *Satellite Remote Sensing for Conservation Action: Case Studies from Aquatic and Terrestrial Ecosystems*; Cambridge University Press: Cambridge, UK, 2018; ISBN 978-1-316-51386-6.
- Tien Bui, D.; Le, K.-T.T.; Nguyen, V.C.; Le, H.D.; Revhaug, I. Tropical Forest Fire Susceptibility Mapping at the Cat Ba National Park Area, Hai Phong City, Vietnam, Using GIS-Based Kernel Logistic Regression. *Remote Sens.* **2016**, *8*, 347. [\[CrossRef\]](#)
- Vilar del Hoyo, L.; Martín Isabel, M.P.; Martínez Vega, F.J. Logistic Regression Models for Human-Caused Wildfire Risk Estimation: Analysing the Effect of the Spatial Accuracy in Fire Occurrence Data. *Eur. J. For. Res.* **2011**, *130*, 983–996. [\[CrossRef\]](#)
- Ghorbanzadeh, O.; Valizadeh Kamran, K.; Blaschke, T.; Aryal, J.; Naboureh, A.; Einali, J.; Bian, J. Spatial Prediction of Wildfire Susceptibility Using Field Survey GPS Data and Machine Learning Approaches. *Fire* **2019**, *2*, 43. [\[CrossRef\]](#)
- Sakellariou, S.; Cabral, P.; Caetano, M.; Pla, F.; Painho, M.; Christopoulou, O.; Sfougaris, A.; Dalezios, N.; Vasilakos, C. Remotely Sensed Data Fusion for Spatiotemporal Geostatistical Analysis of Forest Fire Hazard. *Sensors* **2020**, *20*, 5014. [\[CrossRef\]](#)

22. Sakellariou, S.; Tampekis, S.; Samara, F.; Flannigan, M.; Jaeger, D.; Christopoulou, O.; Sfougaris, A. Determination of Fire Risk to Assist Fire Management for Insular Areas: The Case of a Small Greek Island. *J. For. Res.* **2019**, *30*, 589–601. [[CrossRef](#)]
23. Bedia, J.; Golding, N.; Casanueva, A.; Iturbide, M.; Buontempo, C.; Gutiérrez, J.M. Seasonal Predictions of Fire Weather Index: Paving the Way for Their Operational Applicability in Mediterranean Europe. *Clim. Serv.* **2018**, *9*, 101–110. [[CrossRef](#)]
24. Karali, A.; Hatzaki, M.; Giannakopoulos, C.; Roussos, A.; Xanthopoulos, G.; Tenentes, V. Sensitivity and Evaluation of Current Fire Risk and Future Projections Due to Climate Change: The Case Study of Greece. *Nat. Hazards Earth Syst. Sci.* **2014**, *14*, 143–153. [[CrossRef](#)]
25. Haines, D.A.; Main, W.A.; Frost, J.S.; Simard, A.J. Fire-Danger Rating and Wildfire Occurrence in the Northeastern United States. *For. Sci.* **1983**, *29*, 679–696. [[CrossRef](#)]
26. Preisler, H.K.; Chen, S.-C.; Fujioka, F.; Benoit, J.W.; Westerling, A.L. Wildland Fire Probabilities Estimated from Weather Model-Deduced Monthly Mean Fire Danger Indices. *Int. J. Wildland Fire* **2008**, *17*, 305–316. [[CrossRef](#)]
27. Matthews, S. A Comparison of Fire Danger Rating Systems for Use in Forests. *Aust. Meteorol. Oceanogr. J.* **2009**, *58*, 41–48. [[CrossRef](#)]
28. Safi, Y.; Bouroumi, A. Prediction of Forest Fires Using Artificial Neural Networks. *Appl. Math. Sci.* **2013**, *7*, 271–286. [[CrossRef](#)]
29. Zhang, Q.; Lin, G.; Zhang, Y.; Xu, G.; Wang, J. Wildland Forest Fire Smoke Detection Based on Faster R-CNN Using Synthetic Smoke Images. *Procedia Eng.* **2018**, *211*, 441–446. [[CrossRef](#)]
30. Jeong, M.; Park, M.; Nam, J.; Ko, B.C. Light-Weight Student LSTM for Real-Time Wildfire Smoke Detection. *Sensors* **2020**, *20*, 5508. [[CrossRef](#)]
31. Srinivas, K.; Dua, M. Fog Computing and Deep CNN Based Efficient Approach to Early Forest Fire Detection with Unmanned Aerial Vehicles. In *Inventive Computation Technologies, Proceedings of the ICICT 2019 Conference, Coimbatore, India, 29–30 August 2019*; Springer: Cham, Switzerland, 2020; Volume 98, pp. 646–652. [[CrossRef](#)]
32. Alexandrov, D.; Pertseva, E.; Berman, I.; Pantiukhin, I.; Kapitonov, A. Analysis of Machine Learning Methods for Wildfire Security Monitoring with an Unmanned Aerial Vehicles. In Proceedings of the 2019 24th Conference of Open Innovations Association (FRUCT), Moscow, Russia, 8–12 April 2019; pp. 3–9. [[CrossRef](#)]
33. Zhang, Q.; Xu, J.; Xu, L.; Guo, H. *Forest Fire Smoke Recognition Based on Convolutional Neural Network*; Atlantis Press: Amsterdam, The Netherlands, 2016; pp. 568–575.
34. Jiao, Z.; Zhang, Y.; Xin, J.; Mu, L.; Yi, Y.; Liu, H.; Liu, D. A Deep Learning Based Forest Fire Detection Approach Using UAV and YOLOv3. In Proceedings of the 2019 1st International Conference on Industrial Artificial Intelligence (IAI), Shenyang, China, 23–27 July 2019; pp. 1–5. [[CrossRef](#)]
35. Cao, Y.; Yang, F.; Tang, Q.; Lu, X. An Attention Enhanced Bidirectional LSTM for Early Forest Fire Smoke Recognition. *IEEE Access* **2019**, *7*, 154732–154742. [[CrossRef](#)]
36. Govil, K.; Welch, M.L.; Ball, J.T.; Pennypacker, C.R. Preliminary Results from a Wildfire Detection System Using Deep Learning on Remote Camera Images. *Remote Sens.* **2020**, *12*, 166. [[CrossRef](#)]
37. Lai, C.; Zeng, S.; Guo, W.; Liu, X.; Li, Y.; Liao, B. Forest Fire Prediction with Imbalanced Data Using a Deep Neural Network Method. *Forests* **2022**, *13*, 1129. [[CrossRef](#)]
38. Zheng, S.; Gao, P.; Wang, W.; Zou, X. A Highly Accurate Forest Fire Prediction Model Based on an Improved Dynamic Convolutional Neural Network. *Appl. Sci.* **2022**, *12*, 6721. [[CrossRef](#)]
39. Bisquert, M.; Caselles, E.; Sánchez-Tomás, J.; Caselles, V. Application of Artificial Neural Networks and Logistic Regression to the Prediction of Forest Fire Danger in Galicia Using MODIS Data. *Int. J. Wildland Fire* **2012**, *21*, 1025–1029. [[CrossRef](#)]
40. Joshi, J.; Sukumar, R. Improving Prediction and Assessment of Global Fires Using Multilayer Neural Networks. *Sci. Rep.* **2021**, *11*, 3295. [[CrossRef](#)] [[PubMed](#)]
41. Kucuk, O.; Sevinc, V. Fire Behavior Prediction with Artificial Intelligence in Thinned Black Pine (*Pinus nigra* Arnold) Stand. *For. Ecol. Manag.* **2023**, *529*, 120707. [[CrossRef](#)]
42. Pais, C.; Miranda, A.; Carrasco, J.; Shen, Z.-J.M. Deep Fire Topology: Understanding the Role of Landscape Spatial Patterns in Wildfire Occurrence Using Artificial Intelligence. *Environ. Model. Softw.* **2021**, *143*, 105122. [[CrossRef](#)]
43. Abdollahi, A.; Pradhan, B. Explainable Artificial Intelligence (XAI) for Interpreting the Contributing Factors Feed into the Wildfire Susceptibility Prediction Model. *Sci. Total Environ.* **2023**, *879*, 163004. [[CrossRef](#)]
44. Saha, S.; Bera, B.; Shit, P.K.; Bhattacharjee, S.; Sengupta, N. Prediction of Forest Fire Susceptibility Applying Machine and Deep Learning Algorithms for Conservation Priorities of Forest Resources. *Remote Sens. Appl. Soc. Environ.* **2023**, *29*, 100917. [[CrossRef](#)]
45. Permana, S.D.H.; Saputra, G.; Arifitama, B.; Yaddarabullah; Caesarendra, W.; Rahim, R. Classification of Bird Sounds as an Early Warning Method of Forest Fires Using Convolutional Neural Network (CNN) Algorithm. *J. King Saud Univ.—Comput. Inf. Sci.* **2022**, *34*, 4345–4357. [[CrossRef](#)]
46. Bartzokas, A.; Lolis, C.; Metaxas, D. A Study on the Intra-annual Variation and the Spatial Distribution of Precipitation Amount and Duration over Greece on a 10 Day Basis. *Int. J. Climatol.* **2003**, *23*, 207–222. [[CrossRef](#)]
47. Spiliotopoulos, M.; Holden, N.M.; Loukas, A. Mapping Evapotranspiration Coefficients in a Temperate Maritime Climate Using the METRIC Model and Landsat TM. *Water* **2017**, *9*, 23. [[CrossRef](#)]
48. Pausas, J.G.; Ribeiro, E. The Global Fire–Productivity Relationship. *Glob. Ecol. Biogeogr.* **2013**, *22*, 728–736. [[CrossRef](#)]
49. Mandal, A.; Nykiel, G.; Strzyżewski, T.; Kochanski, A.; Wrońska, W.; Gruszczynska, M.; Mariusz, F. High-Resolution Fire Danger Forecast for Poland Based on the Weather Research and Forecasting Model. *Int. J. Wildland Fire* **2021**, *31*, 149–162. [[CrossRef](#)]

50. Saha, S.; Moorthi, S.; Pan, H.-L.; Wu, X.; Wang, J.; Nadiga, S.; Tripp, P.; Kistler, R.; Woollen, J.; Behringer, D.; et al. The NCEP Climate Forecast System Reanalysis. *Bull. Am. Meteorol. Soc.* **2010**, *91*, 1015–1058. [[CrossRef](#)]
51. Caraballo-Vega, J.A.; Carroll, M.L.; Neigh, C.S.R.; Wooten, M.; Lee, B.; Weis, A.; Aronne, M.; Alemu, W.G.; Williams, Z. Optimizing WorldView-2, -3 Cloud Masking Using Machine Learning Approaches. *Remote Sens. Environ.* **2023**, *284*, 113332. [[CrossRef](#)]
52. Tarpley, J.D.; Schneider, S.R.; Money, L.R. Global Vegetation Indices from the NOAA-7 Meteorological Satellite. *J. Appl. Meteorol. Climatol.* **1984**, *23*, 491–494. [[CrossRef](#)]
53. Kogan, F.N. Droughts of the Late 1980s in the United States as Derived from NOAA Polar-Orbiting Satellite Data. *Bull. Am. Meteorol. Soc.* **1995**, *76*, 655–668. [[CrossRef](#)]
54. Kogan, F.N. Application of Vegetation Index and Brightness Temperature for Drought Detection. *Adv. Space Res.* **1995**, *15*, 91–100. [[CrossRef](#)]
55. McFeeters, S.K. The Use of the Normalized Difference Water Index (NDWI) in the Delineation of Open Water Features. *Int. J. Remote Sens.* **1996**, *17*, 1425–1432. [[CrossRef](#)]
56. Kambezidis, H.D.; Kalliampakos, G.K. Fire-Risk Assessment in Northern Greece Using a Modified Fosberg Fire-Weather Index That Includes Forest Coverage. *Int. J. Atmos. Sci.* **2016**, *2016*, 8108691. [[CrossRef](#)]
57. Van Wagner, C.E. *Development and Structure of the Canadian Forest Fire Weather Index System*; Canadian Forestry Service: Ottawa, ON, Canada, 1987; Volume 35, ISBN 978-0-662-15198-2.
58. Ntinopoulos, N.; Spiliotopoulos, M.; Vasiliades, L.; Mylopoulos, N. Contribution to the Study of Forest Fires in Semi-Arid Regions with the Use of Canadian Fire Weather Index Application in Greece. *Climate* **2022**, *10*, 143. [[CrossRef](#)]
59. Karouni, A.; Daya, B.; Bahak, S. Forest Fire Prediction: A Comparative Study of Applicability of Fire Weather Indices for Lebanon Allowing to Predict a Forest Fire. *J. Commun. Comput.* **2013**, *11*, 1403–1409.
60. Kogan, F.N. Operational Space Technology for Global Vegetation Assessment. *Bull. Am. Meteorol. Soc.* **2001**, *82*, 1949–1964. [[CrossRef](#)]
61. Domenikiotis, C.; Spiliotopoulos, M.; Tsiros, E.; Dalezios, N.R. Early Cotton Yield Assessment by the Use of the NOAA/AVHRR Derived Vegetation Condition Index (VCI) in Greece. *Int. J. Remote Sens.* **2004**, *25*, 2807–2819. [[CrossRef](#)]
62. Kogan, F.N. Remote Sensing of Weather Impacts on Vegetation in Non-Homogeneous Areas. *Int. J. Remote Sens.* **1990**, *11*, 1405–1419. [[CrossRef](#)]
63. Masitoh, F.; Rusydi, A.N. Vegetation Health Index (VHI) Analysis during Drought Season in Brantas Watershed. *IOP Conf. Ser. Earth Environ. Sci.* **2019**, *389*, 012033. [[CrossRef](#)]
64. Yadav, R.; Tripathi, S.; Gogumalla, P.; Dubey, S. Trend Analysis by Mann-Kendall Test for Precipitation and Temperature for Thirteen Districts of Uttarakhand. *J. Agrometeorol.* **2014**, *16*, 164. [[CrossRef](#)]
65. Kartsios, S.; Karacostas, T.; Pytharoulis, I.; Dimitrakopoulos, A.P. Numerical Investigation of Atmosphere-Fire Interactions during High-Impact Wildland Fire Events in Greece. *Atmos. Res.* **2021**, *247*, 105253. [[CrossRef](#)]
66. Edwards, J.; Hakobyan, M.; Lin, A.; Golden, C. Predicting Forest Fires in Madagascar. Available online: https://projects.iq.harvard.edu/files/cs288/files/madagascar_fires.pdf (accessed on 15 December 2022).
67. Al-Kahlout, M.M.; Ghaly, A.M.A.; Mudawah, D.Z.; Abu-Naser, S.S. Neural Network Approach to Predict Forest Fires Using Meteorological Data. *Int. J. Eng. Inf. Syst. (IJEAIS)* **2020**, *4*, 68–72.
68. Wu, Z.; Wang, B.; Li, M.; Tian, Y.; Quan, Y.; Liu, J. Simulation of Forest Fire Spread Based on Artificial Intelligence. *Ecol. Indic.* **2022**, *136*, 108653. [[CrossRef](#)]
69. Pinto, M.M.; DaCamara, C.C.; Hurduc, A.; Trigo, R.M.; Trigo, I.F. Enhancing the Fire Weather Index with Atmospheric Instability Information. *Environ. Res. Lett.* **2020**, *15*, 0940b7. [[CrossRef](#)]
70. Velizarova, E.; Nedkov, R.; Molla, I.; Zaharinova, M. Application of aerospace data for forest fire risk assessment and prognoses. A case study for Vitosha mountain. *Ecol. Eng. Environ. Prot.* **2017**, *VIII*, 38–45. [[CrossRef](#)]
71. Gabban, A.; San-Miguel-Ayanz, J.; Viegas, D. A Comparative Analysis of the Use of NOAA-AVHRR NDVI and FWI Data for Forest Fire Risk Assessment. *Int. J. Remote Sens.* **2008**, *29*, 5677–5687. [[CrossRef](#)]
72. Bugalho, L.; Camara, N.; Kogan, F. Study of Wildfire Environmental Conditions in Portugal with NOAA/NESDIS Satellite-Based Vegetation Health Index. *J. Agric. Sci. Technol. B* **2019**, *9*, 165–174. [[CrossRef](#)]
73. Chéret, V.; Denux, J.-P. Analysis of MODIS NDVI Time Series to Calculate Indicators of Mediterranean Forest Fire Susceptibility. *GISci. Remote Sens.* **2011**, *48*, 171–194. [[CrossRef](#)]
74. Talucci, A.C.; Meigs, G.W.; Knudby, A.; Krawchuk, M.A. Fire Severity and the Legacy of Mountain Pine Beetle Outbreak: High-Severity Fire Peaks with Mixed Live and Dead Vegetation. *Environ. Res. Lett.* **2022**, *17*, 124010. [[CrossRef](#)]
75. Abdollahi, M.; Islam, T.; Gupta, A.; Hassan, Q. An Advanced Forest Fire Danger Forecasting System: Integration of Remote Sensing and Historical Sources of Ignition Data. *Remote Sens.* **2018**, *10*, 923. [[CrossRef](#)]
76. Leblon, B.; Alexander, M.; Chen, J.; White, S. Monitoring Fire Danger of Northern Boreal Forests with NOAA-AVHRR NDVI Images. *Int. J. Remote Sens.* **2001**, *22*, 2839–2846. [[CrossRef](#)]
77. Chen, M.; Tan, Y. SF-FWA: A Self-Adaptive Fast Fireworks Algorithm for Effective Large-Scale Optimization. *Swarm Evol. Comput.* **2023**, *80*, 101314. [[CrossRef](#)]
78. Dulebenets, M.A. An Adaptive Polyploid Memetic Algorithm for Scheduling Trucks at a Cross-Docking Terminal. *Inf. Sci.* **2021**, *565*, 390–421. [[CrossRef](#)]

79. Pasha, J.; Nwodu, A.L.; Fathollahi-Fard, A.M.; Tian, G.; Li, Z.; Wang, H.; Dulebenets, M.A. Exact and Metaheuristic Algorithms for the Vehicle Routing Problem with a Factory-in-a-Box in Multi-Objective Settings. *Adv. Eng. Inform.* **2022**, *52*, 101623. [[CrossRef](#)]
80. Gholizadeh, H.; Fazlollahtabar, H.; Fathollahi-Fard, A.M.; Dulebenets, M.A. Preventive Maintenance for the Flexible Flowshop Scheduling under Uncertainty: A Waste-to-Energy System. *Environ. Sci. Pollut. Res.* **2021**. [[CrossRef](#)] [[PubMed](#)]
81. Dulebenets, M.A. A Diffused Memetic Optimizer for Reactive Berth Allocation and Scheduling at Marine Container Terminals in Response to Disruptions. *Swarm Evol. Comput.* **2023**, *80*, 101334. [[CrossRef](#)]
82. Singh, E.; Pillay, N. A Study of Ant-Based Pheromone Spaces for Generation Constructive Hyper-Heuristics. *Swarm Evol. Comput.* **2022**, *72*, 101095. [[CrossRef](#)]
83. Shtovba, S. Ant Algorithms: Theory and Applications. *Program. Comput. Softw.* **2005**, *31*, 167–178. [[CrossRef](#)]

Disclaimer/Publisher's Note: The statements, opinions and data contained in all publications are solely those of the individual author(s) and contributor(s) and not of MDPI and/or the editor(s). MDPI and/or the editor(s) disclaim responsibility for any injury to people or property resulting from any ideas, methods, instructions or products referred to in the content.